Eur. Phys. J. Special Topics **224**, 2855–2866 (2015)

DOI: 10.1140/epjst/e2015-02593-5

THE EUROPEAN PHYSICAL JOURNAL SPECIAL TOPICS

Regular Article

Effect of boundary conditions on piezoelectric buckled beams for vibrational noise harvesting

F. Cottone, M. Mattarelli, H. Vocca, and L. Gammaitoni

NiPS Laboratory, Dipartimento di Fisica e Geologia, Università di Perugia, 06123 Perugia, Italy

Received 22 August 2015 / Received in final form 9 September 2015
Published online 20 November 2015

Abstract. Nonlinear bistable systems have proven to be advantageous for energy harvesting of random and real ambient vibrations. One simple way of implementing a bistable transducer is setting a piezoelectric beam in a post-buckled configuration by axial compression. Besides, hinged or clamped-clamped type of boundary conditions correspond to two different post-buckled shape functions. Here we study, through theoretical analysis and numerical simulations, the efficiency of a hinged and clamped-clamped piezoelectric bridge under band-limited random noise with progressive axial load. Clamped configuration results to harvest 26% more power than hinged around an optimal axial load of 0.05%, while, in the intra-well trapped situation, above 0.1%, the two configurations present no substantial difference. Nevertheless, simulations confirm the advantage of exploiting inter-well oscillations in bistable regime.

1 Introduction

In last decade, piezoelectric generators have attracted a growing interest of academics and industry because of their employ in vibration energy harvesting as well as in micro- and nano-sensors. The progress in minimization and power consumption of wireless electronics is now reaching the capability of small energy harvesting systems. In fact, the marriage between *zero-power electronics* and energy harvesting systems will enable a vast number of applications of wireless-sensor-network (WSNs), otherwise impossible without self-powering and maintenance-free capabilities [1,2]. This technological improvement is taking place at various physical levels: materials, efficient design, components and circuitry [3,4].

In general, resonating vibration energy harvesters (VEHs) work optimally when the input vibration is tuned to their main frequency, whereas are inefficient far off this value. On the other hand, real ambient vibrations often present variable power spectral density and amplitude in time [2]. Therefore, alternative concepts have been proposed beyond linear spring-mass systems. Some of recent examples are self-tuning systems [5,6], array of oscillators to covers larger frequency interval [7,8] and multimodal oscillators [9,10]. In addition, the exploitation of nonlinear bistable oscillators have been proposed both for electromagnetic transduction [11,12] and via piezoelectric generators by the authors of this work [13,14] and [15,16]. In these works,

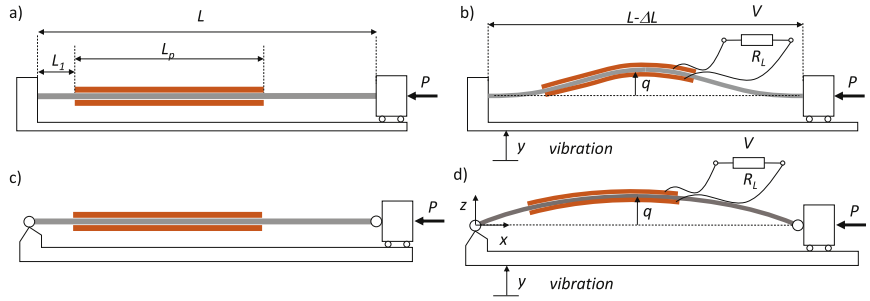

Fig. 1. Piezoelectric beam in unbuckled a) clamped-clamped, c) hinged boundary conditions and b),d) post-buckled configurations with wiring scheme.

a repulsive magnetic force was used to create a Duffing-like potential. However, the use of magnetic fields to induce bistability can interfere with wireless electronics and face complex integration of permanent magnets at small scales. Thus, the employ of bistable piezoelectric buckled beam is more desirable. A theoretical analysis and experiments of piezoelectric buckled beams (PBBs) was previously presented by the author of this work [17] for noise energy harvesting. In this regard, other researchers have studied simply-supported PBBs under harmonic sweeping [18,19]. Buckled piezoelectric bridge were also successfully proposed for air-flow energy harvesting [20]. The enhancement in harvesting performance of buckled configurations have been proven in these works. In particular, these harvesters take advantage from wideband inter-well and intra-well oscillations.

As a further contribution to the understanding of such devices, here we present theoretical analysis and numerical simulations of a unimorph PBB focused on the aspect of different clamping configuration: clamped-clamped (CC) and hinged (HI). The model parameters of the piezoelectric bridge is based on the experimental test device of our previous work [17] and tested under band-limited exponentially correlated vibration noise. The performance comparison is discussed accounting on the symmetry of the piezoelectric layer ratio of time constants of mechanical and electrical branches of the harvester. The electrical and dynamical response have been studied with variable axial compression ratio in order to distinguish mono- and bi-stable regimes.

2 Theoretical model

Here we do not aim at giving a complete analysis, which has been already carried on in [17,21] based on the first order composite plate theory according to Reddy [22]. Nevertheless, we want to investigate the effect of two different boundary conditions of the beam: clamped-clamped and hinged. A sketch of the piezoelectric buckled beam is shown in Fig. 1 in (a) clamped-clamped and (b) hinged setting, whereas Fig. 1(c) represents the post-buckled shape when applying an axial load P. It consists of a support steel beam that can be sandwiched between two (bimorph) or one (unimorph) piezoelectric layer, assumed to be polarized only along the z-axis. An additional inertial mass can be attached onto the mid-point of the beam in order to change the system inertia. One of the extremes is displaced by an amount ΔL, corresponding to a static axial force P. The piezoelectric layer of length L_p starts at a distance L_1 from the left end side. The charges are collected by two electrodes along the piezoelectric layer and short-circuited to a resistive load by wires. The support frame vibrates vertically by a displacement y, and, the shape function $w(x,t)$ of the beam deflection is in general

time dependent. For slender beam, the main contribution to the electro-mechanical coupling is related to the longitudinal strain of the beam, therefore we consider only the effect of e_{zx} in the stress-charge piezoelectric equations.

Considering only the first mode of the Galerkin expansion, $\psi(x)$, the shape function can be expressed as $w(x,t) = \psi(x)q(t)$, where $q(t)$ is the midpoint displacement. By naming V the generated voltage across the electrical load R_L, the Lagrangian $\mathcal{L}(q, \dot{q}, V)$ is:

$$\mathcal{L}(q,\dot{q},V) = \frac{C_p' V^2}{2} - k_0 q V - \frac{1}{2}q^2(k_2 - k_1 V) - k_3 q^3 - \frac{k_4 q^4}{4} + \frac{1}{2}\dot{y}^2(M_0 + M_B) + \frac{1}{2}\dot{q}^2(M_0 + M_{Beff}) + \eta\dot{q}\dot{y} \tag{1}$$

where the overhead dot are time derivatives. The parameters M_0, M_B, M_{Beff} and η represent the mid-point additional mass, total beam mass, effective beam mass and inertia factor respectively; k_0, k_1, k_2, k_3 and k_4 represent, in order, the piezoelectric coupling factor, in-plane piezoelectric force factor, linear, nonlinear cubic and quartic stiffness constant respectively. All these parameters are calculated from physical system characteristics as follows, where the apex are space derivative with respect to x.

$$M_B = b\left(n_S L_p h_p \rho_p + L h_s \rho_s\right), \tag{2}$$

$$\eta = M_0\,\psi(L/2) + n_S L_p h_p \rho_p \int_{L_1}^{L_1+L_p} \psi\, dx + L h_s \rho_s \int_0^L \psi\, dx, \tag{3}$$

$$M_{Beff} = n_S h_p \rho_p \int_{L_1}^{L_1+L_p} \psi^2 dx + h_s \rho_s \int_0^L \psi^2 dx, \tag{4}$$

$$k_0 = \frac{1}{V}\int_{L_1}^{L_1+L_p} M_p(x)\psi'' dx, \tag{5}$$

$$k_1 = \frac{1}{VL}\int_0^L N_p(x)dx \int_0^L (\psi')^2\, dx, \tag{6}$$

$$k_2 = \int_0^L D(x)\,(\psi'')^2\, dx - P\int_0^L (\psi')^2\, dx, \tag{7}$$

$$k_3 = -\frac{1}{2L}\int_0^L (\psi')^2\, dx \int_0^L B(x)\psi''\, dx, \tag{8}$$

$$k_4 = \frac{1}{2L^2}\int_0^L A(x)dx \left(\int_0^L (\psi')^2\, dx\right)^2. \tag{9}$$

These expressions are valid for piezoelectric layers that are not, in general, symmetrically placed with respect the midpoint of the support layer.

The difference between unimorph to bimorph beams and series and parallel configuration depends on the parameters: n_s, A, B, D, N_p, M_p; where, n_s is the number

of piezoelectric layers (1 for unimorph, 2 for bimorph), A, B, D represent the stiffness of the beam to, respectively, extensional, mixed bending-extensional and bending stiffness. In a isotropic material they are the first three moments of Young modulus. Because of symmetry along z-axis, $B = 0$ for bimorph beams. N_p, M_p are the piezoelectric resultants and depend also on the electrical connection: for bimorph beams connected in series (parallel) $N_p = 0$ ($M_p = 0$). Moreover, for first order Galerkin expansion, the k_0 component reduces up to zero as L_p tends to L.

The Euler-Lagrange equations obtained from Eq. (1), in the generalized coordinates of the beam midpoint, result

$$(M_0 + M_{BEff})\,\ddot{q} + c\dot{q} + k_2 q + 3k_4 q^2 + k_3 q^3 + (k_0 - k_1 q)\,V = -\eta\ddot{y} \tag{10}$$

$$C_p \dot{V} + \frac{V}{R_L} = k_0 \dot{q} - k_1 q \dot{q} \tag{11}$$

having considered the mechanical dissipation as $(c\dot{q})$. The vibration source transfers energy to the system through the inertial force $\eta\ddot{y}$.

2.1 Differences between hinged and clamped configuration

The boundary conditions on the shape function $w(x,t)$ depends on the physical connections at the extremes, in particular, $w(0) = w(L) = w'(0) = w'(L) = 0$ for clamped and $w(0) = w(L) = w''(0) = w''(L) = 0$ for hinged configuration. Therefore, considering only the first mode ψ of Galerkin expansion, the shape function takes the form $w(x,t) = \psi(x)q(t)$ with

$$\psi_H = sin\left(\frac{\pi x}{L}\right), \qquad hinged \tag{12}$$

$$\psi_C = \frac{1 - cos\left(\frac{2\pi x}{L}\right)}{2}, \qquad clamped. \tag{13}$$

From a direct inspection, we expect no differences in terms involving the integral of $(\psi\prime)^2$ and only a multiplicative factor close to 1 in terms involving ψ and $(\psi\prime\prime)^2$. In particular k_1 and k_4 are unaffected, while η and M_{Beff} are always larger in the hinged system. In reality, these differences are not really significant in presence of the additional mass M_0 as, usually, it dominates over M_{Beff}. In our case $M_0/M_{Beff} = 4.7$. The term k_2, which would depend on the kind of support, is modulated by the external axial force, P. The critical buckling load, beyond which k_2 becomes negative, P has to be larger in clamped configuration [22].

The terms which are significantly dependent on the hinged/clamped state are k_3 and k_0. The k_3 term, present only for unimorph systems, accounts for the preferential buckling of the beam toward the less stiff side. Depending on the difference between the Young moduli, it can strongly affects the dynamical behaviour of not-buckled beams, but in *deeply* buckled systems it is negligible. More important is the effect on the first electromechanical coefficient k_0 (the second being k_1). Note that this means that for parallel connected bimorph beams which have $M_p = 0$, there is no practical difference with the clamping scheme.

On the contrary, for bimorph, series connected systems $k_1 = 0$, and therefore the coupling of the electrical circuit with the mechanical vibration depends only on k_0. In order to maximize k_0, the design of the beam should be different for clamped and hinged beams: in particular the length of the piezoelectric layers L_p, should be equal

Table 1. Values of the electromechanical coupling coefficient for bridged beams.

	Clamped	Hinged
Bimorph Series	k_0 max if $L_1 = L/4$ and $L_p = L/2$ $k_1 = 0$	k_0 max if $L_p = L$ $k_1 = 0$
Bimorph Par	$k_0 = 0$ k_1 max if $L_p = L$	$k_0 = 0$ k_1 max if $L_p = L$
Unimorph	k_0 max if $L_1 = L/4$ and $L_p = L/2$ k_1 max if $L_p = L$	k_0 max if $L_p = L$ k_1 max if $L_p = L$

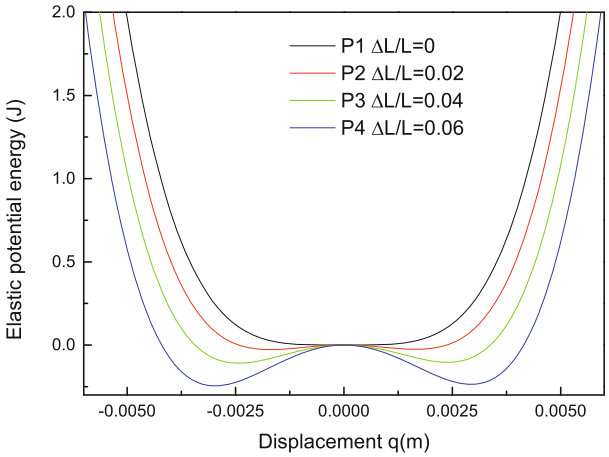

Fig. 2. Elastic potential energy of the piezoelectric beam as a function of mid-point displacement for increasing values of axial compression ratio $\Delta L/L$. The potential parameters have been computed using the data in Table 2.

to the total length L or $L/2$ respectively for hinged or clamped beams, with k_0 taking the value $\pi b\, e_{zx}(h_s + h_p)/L$ in both cases.

In unimorph beams, in principle, both k_0 and k_1 can be different from zero at the same time. Still, holding the previous considerations on k_0, in the clamped configuration, it is not possible to maximize both k_0 (maximum at $Lp = L/2$) and k_1 (maximum at $Lp = L$). Note that in any case in the unimorph beams there is a higher degree of complexity.

Table 1 summarizes the values taken by the electromechanical parametrs k_0 and k_1 for the cases just discussed.

2.2 Potential energy

The potential energy (at short circuit) is represented in Fig. 2 for increasing values of $\Delta L/L = 0 \div 0.06$. The critical buckling load P_{cr} corresponds to $k_2 = 0$, hence, by equating to zero Eq. (7),

$$P_{cr} = \int_0^L D(x)\,(\psi'')^2\,dx \Big/ \int_0^L (\psi')^2\,dx. \tag{14}$$

For $P \leq P_{cr}$, $k2 \geq 0$ and the potential energy is a quartic with one global minimum $q_0 = 0$. For $P > P_{cr}$, $k_2 < 0$ and the Duffing-like potential has two local minima

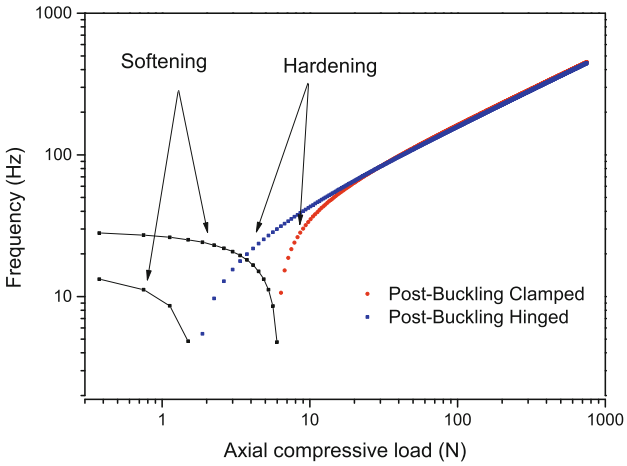

Fig. 3. Oscillation frequency around local minima versus increasing values of the axial load P corresponding to $\Delta L/L = 0 \div 0.33\%$.

q_- and q_+

$$q_- = \frac{-3k_3 - \sqrt{9k_3^2 - 4k_2k_4}}{2k_4}, \quad q_+ = \frac{-3k_3 + \sqrt{9k_3^2 - 4k_2k_4}}{2k_4}. \tag{15}$$

In the unimorph case, the cubic term k_3 is not zero, hence, the potential function is, in fact, slightly tilted. As the axial load P increases, the beam dynamics spans from monostable to bistable, depending on the noise amplitude and potential barrier. In particular, for increasing axial load close to critical buckling, the potential well is flattened and the resonant frequency decreases, which results in *softening effect*; whereas, above the critical buckling load the oscillation frequency around the two potential minima increases resulting in *hardening effect*. This effect can be seen by computing the local oscillation frequency around the equilibrium positions q_- and q_+

$$f_- = \frac{1}{2\pi}\sqrt{\frac{-k_2 + 3k_3q_-}{M_0 + M_{Beff}}}, \quad f_+ = \frac{1}{2\pi}\sqrt{\frac{-k_2 - 3k_3q_+}{M_0 + M_{Beff}}}. \tag{16}$$

It can be noted that, when the beam is unbuckled we have only one equilibrium position $q_0 = q_- = q_+ = 0$, hence, the resulting resonance becomes the one of the linear oscillator $f_0 = \sqrt{k_2/(M_0 + M_{Beff})}/2\pi$. In addition, when the beam is bimorph, $k_3 = 0$ and the local minima retrieve back to those of symmetric quartic potential as in [17].

Figure 3 shows the oscillation frequency around q_+ as a function of the axial load calculated by Eq. (16) for both clamped and hinged case. The *softening* effect is clear when the compression approaches the critical buckling, whereas the *hardening* takes place beyond this value. As expected, the critical buckling load is higher for clamped than hinged configuration, due to the higher stiffness of the former.

3 Numerical simulations

The case of unimorph beam is of particular interest because the electromechanical terms k_0 and k_1 are both not zero, as well as the asymmetrical elastic contribution

Table 2. Model parameters used for numerical simulations. The chosen piezoelectric material was Lead-Zirconate-Titanate (PZT).

Parameter, symbol	Value
Support layer	
Young's modulus, E_s	200 GPa
Mass density, ρ_s	$7850\,\mathrm{kgm}^{-3}$
Length, L	60×10^{-3} m
Width, b_s	10×10^{-3} m
Thickness, h_s	0.1×10^{-3} m
Piezoelectric layer (PZT)	
Young's modulus, E_p	62 GPa
Mass density, ρ_p	$7800\,\mathrm{kgm}^{-3}$
Length, L_p	30×10^{-3} m
Width, b_p	10×10^{-3} m
Thickness, h_s	0.08×10^{-3} m
Distance from end, L_1	10×10^{-3} m
Relative permittivity, ε_r	3800
Piezoelectric constant, e_{31}	$-6.2\,\mathrm{C\,m}^{-1}$

given by k_3. Therefore, in the following we will focus on this configuration. Moreover, we choose a piezoelectric layer placed on top of the steel support symmetrically centered around the midpoint in order to maximize k_0. In particular, we will study the dependence of the harvested power on the design of a unimorph piezoelectric beam in clamped and hinged boundary conditions with parameters calculated as reported in the Appendix. Table 2 resumes the physical parameters used for the model under consideration. Note that the length of the piezolectric layer was chosen in order to maximize k_0 for the clamped configuration. Numerical simulations were performed under exponentially correlated Gaussian noise with base acceleration amplitude of $\sigma = 1 g_{rms}$, correlation time of $\tau = 0.001$ s and damping term $c = 0.05\,\mathrm{Nsm}^{-1}$. The nonlinear stochastic Eqs. (10) and (11) were integrated by using the modified Euler method with predictor-corrector [23,24]. In particular, the time evolution of the mid-point displacement $q(t)$ and voltage $V(t)$ across a load R_L =10 kΩ were performed for increasing values of compression ratio $\Delta L/L$ in order to scan the dynamics going from monostable to bistable regime.

Figure 4 shows the time traces of the mid-point displacement $q(t)$ and voltage $V(t)$ across an electrical load of 10 kΩ for (right) clamped and (left) hinged configuration at compressive ratio of $\Delta L/L = 0.1\%$. It can be noted that clamped beam seems to snap across the barrier height a bit more frequently than hinged, though, the resulting maximum displacement is almost equal. In both cases, one of the potential minima seem to be slightly preferred. However, this asymmetry, that is due to the cubic term of the potential, is very mild as expected. The resulting RMS voltage is comparable in both cases: 7.5 V (clamped) and 7.3 V (hinged). Even if the acceleration base is the same in the two cases, clamped beam is, indeed, a bit more stressed close to its ends than hinged one. In addition, there is a difference in the electromechanical coupling: $k_0 = 3.2 \times 10^4$ (clamped), while, $k_0 = 2.3 \times 10^4$ (hinged).

In Fig. 5 we can see the behavior of the midpoint displacement standard deviation, $\sigma(q)$, and generated voltage, RMS(V) versus $\Delta L/L$, calculated over a time evolution of 10 s, with an integration step $dt = 10^{-5}$ s. Starting by zero compression, the PBBs oscillation increases around the equilibrium position, then, after passing the critical bucking, snap through the barrier of the potential well and reach a maximum amplitude, which results 1.08 mm for clamped and about 0.9 mm for hinged. After

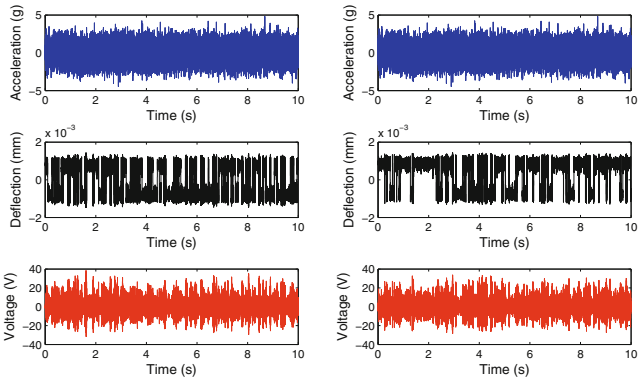

Fig. 4. Numerical simulations of the piezoelectric beam in post-buckled configuration with $\Delta L/L = 0.05\%$ and $R_L = 10\,\mathrm{k}\Omega$. From top to bottom: input base acceleration (exponentially correlated Gaussian noise of $\sigma = 1 g_{\mathrm{rms}}$), mid-point displacement and output voltage across electrical load, for (left-column) clamped and (right-column) hinged.

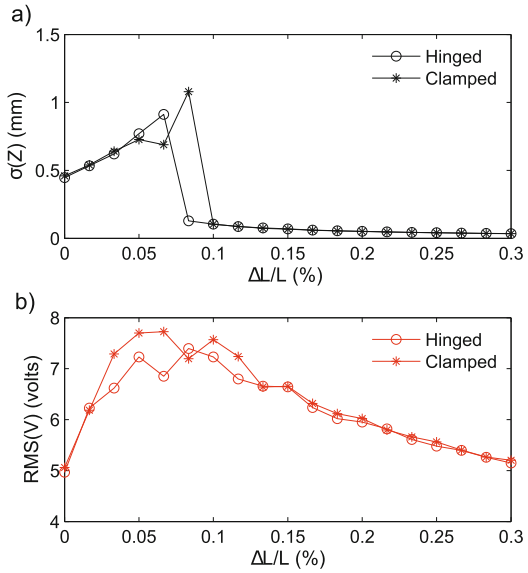

Fig. 5. (a) Standard deviation of mid-point displacement and (b) RMS voltage across load versus axial compression ratio $\Delta L/L = 0 \div 0.3\%$ at $1 g_{rms}$ of base acceleration and $R_L = 10\,\mathrm{k}\Omega$.

a certain axial load, depending on the vibration amplitude and Kramers rate [25], the inter-well jumps cease and the beam vibrates around one of the local minima. What is interesting to note, is that the region of the maximum voltage anticipates the max displacement over the axial load increase. The optimal working point for the max power is thus located in the inter-well region, but it does not necessarily correspond to the max amplitude of oscillation. Furthermore, the clamped beam shows a max $V_{rms} = 7.7$, while for the hinged $V_{rms} = 7.2$, and, below 0.13%, little higher performance in the bistable regime of inter-well oscillations.

In the intra-well region, the oscillation amplitudes and RMS voltage converge for the two configurations. In addition, the RMS voltage doesn't fall down in this region along with the displacement, as it was shown in [17,19] because of the presence of

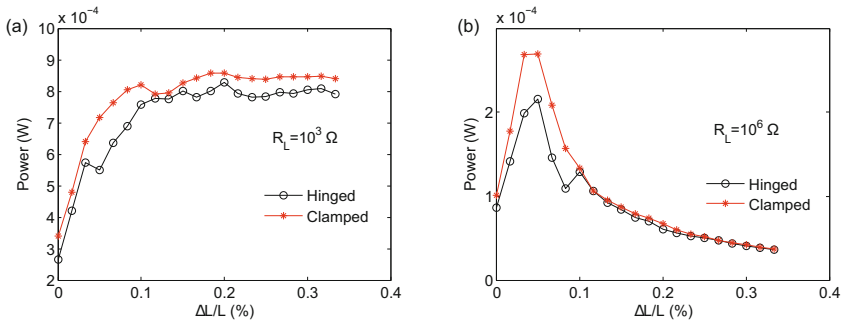

Fig. 6. Generated power for hinged and clamped configurations versus axial compression ratio $\Delta L/L = 0 \div 0.3\%$ for two different electrical load: (a) $R_L = 10^3\,\Omega$ and (b) $R_L = 10^6\,\Omega$ at $1g_{rms}$.

higher harmonics (stiffening effect), well above the cut-off frequency of the the circuit, that compensate the lower displacement amplitude.

3.1 Power performance

Now, we want to analyze the power performance for different electrical time scales determined by the value of $\tau_c = R_L C$. In particular, when this value approached zero or infinite, in order to analyze the efficiency of nonlinearity, as was also shown by Halvorsen [26].

In Fig. 6 the average power $P = < V^2 > /R_L$ is calculated for two different values of electrical load: (left) $R_L = 10^3$ and (right) $R_L = 10^6$. These values yield two characteristic times of equivalent circuit: $\tau_c = 6 \times 10^{-2}$ s and $\tau_c = 6 \times 10^{-5}$ s, and the related cut-off frequencies of the high-pass filter result $f_c = 1/(2\pi\tau_c) = 2.5\,\text{Hz}$ and $2.5\,\text{kHz}$. As a consequence, the ratio between mechanical (Eq. (16)) and cut-off frequency is $f_{+/-}/f_c > 1$ and $f_{+/-}/f_c < 1$, which means that, in the first case (a),(c), the harvester takes advantage of the wide bandwidth of the bistable regime, whereas, in the second case (b),(d), only higher harmonics of the intra-well oscillations contribute to the generation of electrical power that are provided at high compression ratio $\Delta L/L = 0.2 \div 0.3\%$. As expected, in the fast time-scale (left-column) the power achieves a plateaux of max value soon after $\Delta L/L = 0.1\%$, whereas, in the slow time-scale (right-column), the maximum power is located around $\Delta L/L = 0.05\%$, in the bistable regime with inter-well oscillations. Finally, here the clamped configuration results about 20% more efficient than the hinged one.

Figure 7 illustrates the comparison of the RMS voltage and the corresponding electrical power versus the electrical load. In particular, the unbuckled beam is compared to a post-buckled configuration with $\Delta L/L = 0.05\%$. The maximum power generated in buckled case is 2 times higher than that of the unbuckled for both hinged and clamped configuration. The optimal load has been found to be $R_{opt} \sim 15\,\text{k}\Omega$ for both systems, at which: the clamped configuration shows a power peak $P_{max} = 6.3\,\text{mW}$, while, for hinged, $P_{max} = 5\,\text{mW}$, thus a difference of 26%.

4 Conclusions

In this work, the theoretical model of a piezoelectric bridge (PZT), based on composite linear plate theory, was analyzed. In particular, the study was focused on the

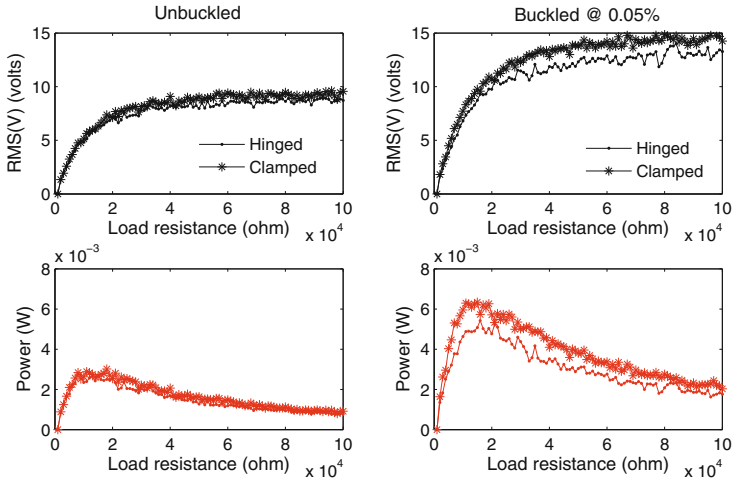

Fig. 7. Top: RMS voltage and (bottom) average power across load for hinged and clamped configurations for axial compression ratio of $\Delta L/L = 0\%$ (unbuckled) and 0.05% (buckled) respectively, at $1g_{rms}$.

effect of different boundary conditions: clamped-clamped and hinged, with progressive axial load. A unimorph piezoelectric beam with symmetric piezoelectric layer was discussed and numerically simulated under transverse vibration generated by exponentially correlated Gaussian noise.

Clamped conguration showed slightly better performance than hinged, with about 26% more generated power, in the bistable regime with inter-well oscillations, corresponding to axial compression $\Delta L/L < 0.1\%$. Above this value, the two configurations converge, so there is no substantial difference.

Regarding to the circuit filtering, for fast circuit time-scale, $\tau_c = R_L C \simeq 6.3 \times 10^{-5}$ s, the generated power achieve a plateux just above 0.1% of axial compression, whereas, for slow circuit time-scale, $\tau_c = R_L C \simeq 6.3 \times 10^{-2}$ s, the optimal efficiency is within 0 and 0.1%.

In conclusion, the results confirm the advantage of exploiting the nonlinear bistable regime for piezoelectric bridge operating as vibrational energy harvester with low damping, and, when choosing the type of support, clamped-clamped ends appear the best choice.

Appendix

Unimorph beam

For a unimorph beam, the electrical and mechanical parameters assume the following values:

$$N_p(x) = be_{zx} V \, \Pi_{L_1}^{L_1+L_p}(x), \tag{A.1}$$

$$M_p(x) = 1/2 be_{zx} h_s V \, \Pi_{L_1}^{L_1+L_p}(x), \tag{A.2}$$

$$A(x) = bE_s h_s + bE_p h_p \, \Pi_{L_1}^{L_1+L_p}(x), \tag{A.3}$$

$$B(x) = -(1/2)bE_s h_p h_s + 1/2bE_p h_p h_s \, \Pi_{L_1}^{L_1+L_p}(x), \tag{A.4}$$

$$D(x) = 1/12b(3E_s h_p^2 h_s + E_s h_s^3) + 1/12b(E_p h_p^3 + 3E_p h_p h_s^2) \, \Pi_{L_1}^{L_1+L_p}(x), \tag{A.5}$$

the step function $\Pi_{L_1}^{L_1+L_p}(x)$ assumes the value 1 between the extremes of piezoelectric layer (L_1 and $L_1 + L_p$) zero otherwise. It is included to account for the x-axis dependency of the coefficients N_p, M_p, A, B and D because the steel and piezoelectric layers have not in general the same length.

This work was supported by European Commission under the EU Horizon 2020 Programme for research, technological development and demonstration (Grant agreement No. 644852, PROTEUS) and under FP7 (Grant agreement No. 611004, ICT-Energy), by Fondazione Cassa di Risparmio di Perugia (Bando a tema Ricerca di Base 2013, Caratterizzazione e micro-caratterizzazione di circuiti MEMS per generazione di energia pulita), and by ONRG grant N00014-11-1-0695.

References

1. H. Vocca, F. Cottone, *ICT – Energy – Concepts Towards Zero – Power Information and Communication Technology* (InTechOpen, February, 2014)
2. P.D. Mitcheson, E.M. Yeatman, G.K. Rao, A.S. Holmes, T.C. Green, Proc. IEEE **96**, 1457 (2008)
3. A. Bilbao, D. Hoover, J. Rice, J. Chapman, Proc. SPIE **7981**, 798109 (2011)
4. S. Meninger, J.O. Mur-Miranda, R. Amirtharajah, A. Chandrakasan, J.H. Lang, IEEE Transactions on Very Large Scale Integration (VLSI) Systems **9**, 64 (2001)
5. C. Eichhorn, R. Tchagsim, N. Wilhelm, P. Woias, J. Micromech. Microengineering **21**, 104003 (2011)
6. I.N. Ayala-Garcia, P.D. Mitcheson, E.M. Yeatman, D. Zhu, J. Tudor, S.P. Beeby, Sensors and Actuators A: Phys. **189**, 266 (2013)
7. D. Koyama, K. Nakamura, Proc. IEEE Ultrasonics Symp., 1973 (2010)
8. M. Ferrari, V. Ferrari, M. Guizzetti, D. Marioli, A. Taroni, Sensors Actuators, A: Phys. **142**, 329 (2008)
9. Y. Tadesse, S. Zhang, S. Priya, J. Intell. Mater. Syst. Struct. **20**, 625 (2009)
10. J. Yang, Y. Wen, P. Li, X. Yue, Q. Yu, X. Bai, Appl. Phys. Lett. **103** (2013)
11. S.G. Burrow, L.R. Clare, A resonant generator with non-linear compliance for energy harvesting in high vibrational environments **1**, 715 (2007)
12. F. Cottone, P. Basset, H. Vocca, L. Gammaitoni, T. Bourouina, J. Intell. Mater. Syst. Struct. **25**, 1484 (2014)
13. F. Cottone, H. Vocca, L. Gammaitoni, Phys. Rev. Lett. **102**, 080601 (2009)
14. L. Gammaitoni, I. Neri, H. Vocca, Appl. Phys. Lett. **94** (2009)
15. A. Erturk, W.G.R. Vieira, C. De Marqui Jr., D.J. Inman, Appl. Phys. Lett. **96**, (2010)
16. S.C. Stanton, C.C. McGehee, B.P. Mann, Physica D: Nonlinear Phenomena **239**, 640 (2010)
17. F. Cottone, L. Gammaitoni, H. Vocca, M. Ferrari, V. Ferrari, Smart Mater. Struct. **21** (2012)
18. R. Masana, M.F. Daqaq, J. Appl. Phys. **111** (2012)
19. C. Xu, Z. Liang, B. Ren, W. Di, H. Luo, D. Wang, K. Wang, Z. Chen, J. Appl. Phys. **114** (2013)
20. C.A. Kitio Kwuimy, G. Litak, M. Borowiec, C. Nataraj, Appl. Phys. Lett. **100**, 2013 (2012)

21. R. Masana, M.F. Daqaq, J. Vibr. Acoustics, Trans. ASME **133** (2011)
22. J.N. Reddy, *Mechanics of laminated composite plates and shells: theory and analysis* (CRC press, 2004)
23. D.J. Higham, SIAM Rev. **43**, 525 (2001)
24. K. Burrage, T. Tian, J. Comput. Appl. Math. **131**, 407 (2001)
25. L. Gammaitoni, F. Marchesoni, E. Menichella-Saetta, S. Santucci, Phys. Rev. Lett. **62**, 349 (1989)
26. E. Halvorsen, Phys. Rev. E – Statistical, Nonlinear, Soft Matter Phys. **87** (2013)